

Adhesive and bending failure of thermal sprayed hydroxyapatite coatings: Effect of nanostructures at interface and crack propagation phenomenon during bending

H. Li ^{a,*}, K.A. Khor ^a, P. Cheang ^b

^a School of Mechanical and Aerospace Engineering, Nanyang Technological University, 50 Nanyang Avenue, Singapore 639798, Singapore

^b School of Chemical and Biomedical Engineering, Nanyang Technological University, 50 Nanyang Avenue, Singapore 639798, Singapore

Received 14 November 2005; received in revised form 25 May 2006; accepted 1 June 2006
Available online 12 July 2006

Abstract

Hydroxyapatite (HA) coatings have shown promising effects on rapid bone remodeling and suitable functional life in orthopedic and dental applications. However, the major problem encountered by the HA-coated implants is the failure of the coating due to its insufficient mechanical properties. The present study investigated the influence of the microstructure near to the coating/substrate interface on the adhesion of the coatings. In addition, the crack propagation behavior within the coatings was studied through 4-point bend test. Results showed that nanostructures (30–110 nm) within the HA coatings were achieved by high velocity oxy-fuel (HVOF) spraying. Comparison among HVOF HA coatings, which were deposited using different starting feedstock, suggests detrimental effect of the perpendicular-to-substrate nano-cuboids on adhesion of the coatings. The presence of the grains with hexagonal shape (<250 nm in length and <50 nm in diameter) triggered a deteriorated adhesion. Granular nanosized grains at the interface give rise to enhanced adhesion through improved mechanical interlocking. Formation mechanism of the nanosized grains was discussed in this paper. Furthermore, the 4-point bend test revealed consistent crack propagation path that the cracks actually grow within the coating with a direction parallel to the interface, and approximately several to 20 microns thick coatings were remained on the substrate. The critical strain energy release rate exhibited a value of $\sim 1.15 \text{ kJm}^{-2}$. During the crack propagation, kinking and trapping of the bending cracks were decided by the flaws within the coating, which were mainly located at splats' interface. The interface between the first layer (with one splat thickness) and the second is believed to be the weakest zone in the nanostructured coating.

© 2006 Elsevier Ltd. All rights reserved.

Keywords: Hydroxyapatite coating; Adhesive failure; Nanostructures; 4-point bending

* Corresponding author. Tel.: +65 6790 4351; fax: +65 6792 4062.
E-mail address: mhli@ntu.edu.sg (H. Li).

1. Introduction

Biomedical application of thermal sprayed hydroxyapatite (HA, $\text{Ca}_{10}(\text{PO}_4)_6(\text{OH})_2$) coatings on metallic implants has been successful since they are capable of promoting new bone ingrowth and apposition. However, the major problems pertaining to the HA-coated implants are their poor long-term functional service due to the failure of the coatings. Extensive studies revealed that the long-term functional performance of the coated implants was influenced significantly by the microstructure of the coatings [1,2]. In addition, HA coating has a potential problem of introducing an additional interface into the implant system. The interface between HA coating and metallic alloy is critical in determining the reliability of the implant [3–7]. Previous studies have reported that fracture often occurred at the HA/substrate interface rather than at the bone/HA interface from a direct shear loading [8–10]. The analysis of malfunctioned dental implants evidenced the failure to be primarily located at HA/metal interface [7]. Consequently, estimation of the interface properties is essential for evaluating the HA coated implants. When used as dental and orthopedic implants, due to identified clinical environment, HA coatings experience compound stresses, which can include shear, bending, tensile and compressive forces. Among all the mechanical performances required, adhesion and fracture toughness are the most critical variables. Besides the adhesive strength, strain energy release rate is also capable of evaluating the interface [11]. The strain energy density theory has been extended to study the growth characteristics of three-dimensional cracks within coatings [12]. Four-point bend test was usually used to determine the strain energy release rate of the coatings at the coating/substrate interface upon the considerations that the interface between the two different materials is usually the weakest part and failure initiated from an interfacial defect was often observed [13–15]. The four-point bend test for evaluating the bonding between coating and substrate has the advantages of providing stresses more like those experienced in vivo of the HA coatings [16].

Furthermore, nanostructured coatings attracted intense interest in recent years due to their enhanced mechanical properties [17–21]. In vitro studies have further reported that nanosized ceramics (Al_2O_3 , TiO_2) possess significant capability of decreasing apoptotic cell death and hence improving cell proliferation [22]. It was proven that nanosized ceramics enhanced osteoblast adhesion on them [23]. Nanostructures within a biocompatible coating could therefore be promising for enhanced bioactivity. However, the knowledge about the influence of the nanostructures on the mechanical properties of the thermal sprayed coatings is yet insufficient so far. In this study, the nanostructured HA coatings have been fabricated. The effect of the nanostructures at the coating/substrate interface on adhesion and bending behavior was studied.

2. Experimental details

In-house synthesized sprayed-dried nanostructured HA powder was utilized for the coating deposition on Ti-6Al-4 V substrates employing high velocity oxy-fuel (HVOF) process. Close examination of the spherical powder particles showed the nanostructures (with rod-like shape grains: <500 nm in length and 40–70 nm in diameter). A nanostructured HA particle was formed by the agglomeration of individual nanosized HA cylindrical grains (the image was not shown in this paper). A fully computerized HV2000 HVOF system (PRAXAIR, USA) with a nozzle diameter of 19 mm was employed for the spraying. The flow rate of the oxygen and hydrogen was 280 l/min and 566 l/min, respectively. The powder feeding gas was purified argon with the flow rate of 19 l/min. The powder feeding rate and spray distance were 8 g/min and 250 mm respectively. The HA powder with different particle size ranges, $50 \pm 10 \mu\text{m}$, $40 \pm 10 \mu\text{m}$, $30 \pm 10 \mu\text{m}$, was sprayed for a purpose of clarifying the influence of melt state of the powder particles on the nanostructural features of resultant coatings. Before coating deposition, degreasing and grit blasting were carried out to make the substrate surface clean and coarse. Alumina sand (250 μm) was utilized to coarsen the substrate surface. The air pressure for the grit-blasting was 4 bar. The roughness of the coarsened Ti6Al4V substrate was around 4.5 μm in Ra as measured using a surface roughness analyzer (Mitutoyo SURF TEST SV-600). Microstructure of the coating samples was analyzed using scanning electron microscopy (SEM, JEOL JSM-5600LV) and field emission SEM (FESEM, JEOL JSM-6700F).

The adhesive bonding strength of the HA coating was measured according to the ASTM C633-79 standard. The universal testing system, Instron 4204, was used for the adhesive strength measurement with the

cross-head speed of 1 mm/min. The coating thickness for the adhesive strength test in the present study was kept at $180 \pm 15 \mu\text{m}$. As discussed, the strain energy release rate is an appropriate variable for evaluating the energy of the inception of cleavage and dislocation emission along the interface. It is essential to relate the resistance of the material to crack propagation to a parameter that can characterize the fracture toughness of the material. With regard to the complex stresses at the coating/substrate interface, it is not easy to get the fracture toughness to represent interface property. Generally used variable as an alternative of the fracture toughness is based on the determination of strain energy release rate, G . For thermal sprayed coatings, the four-point bend test was believed to be an effective technique for the determination of critical strain energy release rate (G_{ss}) at the coating/substrate interface [15,24]. The specimen loaded by 4-point bend for the G_{ss} determination is schematically depicted in Fig. 1.

G can be obtained from the strain energy, U , per unit cross section according to beam theory under plane strain conditions,

$$G = \frac{\partial U}{\partial a} \quad (1)$$

where a is the propagated crack length. G_{ss} during crack propagation can be expressed in the non-dimensional form [25,26]:

$$G_{ss} = \frac{M^2(1 - \nu_2^2)}{2E_2} \left(\frac{1}{I_2} - \frac{\lambda}{I_c} \right) \quad (2)$$

where E is the Young's modulus, I is the inertia moment, ν is Poisson's ratio, and

$$M = Pl/2b \quad (3)$$

$$\lambda = E_2(1 - \nu_1^2)/E_1(1 - \nu_2^2) \quad (4)$$

$$I_c = h_1^3/12 + \lambda h_2^3/12 + \lambda h_1 h_2 (h_1 + h_2)^2/4(h_1 + \lambda h_2) \quad (5)$$

$$I_2 = h_2^3/12 \quad (6)$$

In order to determine G_{ss} , both the applied load and the displacement of the loading points were continuously monitored and recorded. The specimen was loaded until both cracks had propagated out to the internal loading points. Stable crack advance should ideally occur at a constant load, whereas a crack burst causes a sharp drop in load between two values having a mean of P_c [14].

For the four-point bend test, it was pointed out that the pre-crack length, a , had a significant effect on G_{ss} [13]. If the specimen dimension satisfies the relation $0.05 \leq h_1/H \leq 0.5$, a steady interfacial crack can be achieved in the extensive crack length range $0.2h_1 \leq a \leq 0.9(c - l)$ [27]. In the present study, the following parameters were used: $2a = 10 \text{ mm}$, $h_1 = 0.320 \text{ mm}$, $h_2 = 1.95 \text{ mm}$, $b = 2 \text{ mm}$, $2c = 80 \text{ mm}$, $l = 20 \text{ mm}$. The pre-crack was prepared through putting a mask on the substrate surface with a width of 5 mm to prevent from

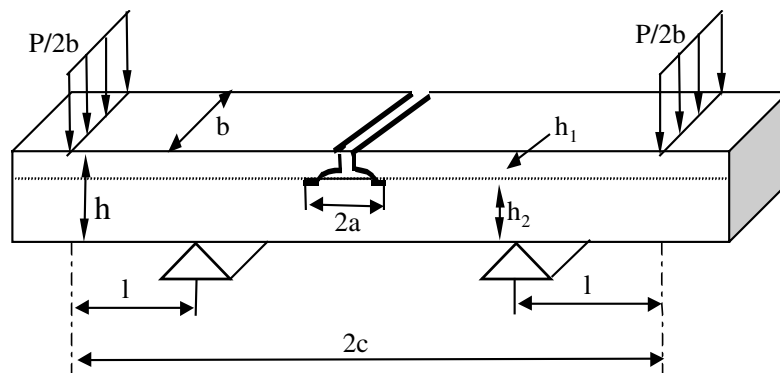


Fig. 1. Schematic depiction of the coating/substrate bimaterial specimen for 4-point bend test (h_1 : coating thickness, h_2 : substrate thickness).

the grit-blasted coarsening. After the coating deposition, a notch was prepared through cutting the coating along its central line using a knife. Subsequently, a three-point bend was performed on the Instron universal-testing machine with a support span of 10 mm to prepare the pre-crack with the length of 10 mm. The bending speed was 1 mm/min. The Young's modulus of the samples employed for the calculation was determined from a 3-point bend test, which has been described in detail previously [28]. The values were 29.01 GPa, 24.82 GPa, and 20.55 GPa for the coatings made from 30 μm , 40 μm , and 50 μm powder.

3. Results and discussion

The HA coatings show clearly the evidence of the presence of nanostructures at both their surfaces and cross-sections (Fig. 2). It was noted that for the HA coatings, grain sizes are different depending on the starting powder sizes (as summarized in Table 1). Similar grain sizes can be seen at both the coating surface and cross-sections. The slight difference might be probably attributed to the melt state of the particles attained during the spraying. It has been found that the measured MFP (defined here as the melting fraction of the particles) values for the particles with the size of 50 μm lies in the range 20–60%. Whilst the particles with the size of 40 μm demonstrate MFP values in the range 40–80%. The 30 μm particles have already fully melted during the spraying. Adhesive test revealed an adhesive strength of up to 31 MPa (Fig. 3). Tensile failure analysis has suggested an entire adhesive failure mode (not shown in this paper), in other word, the failure took place at the coating/

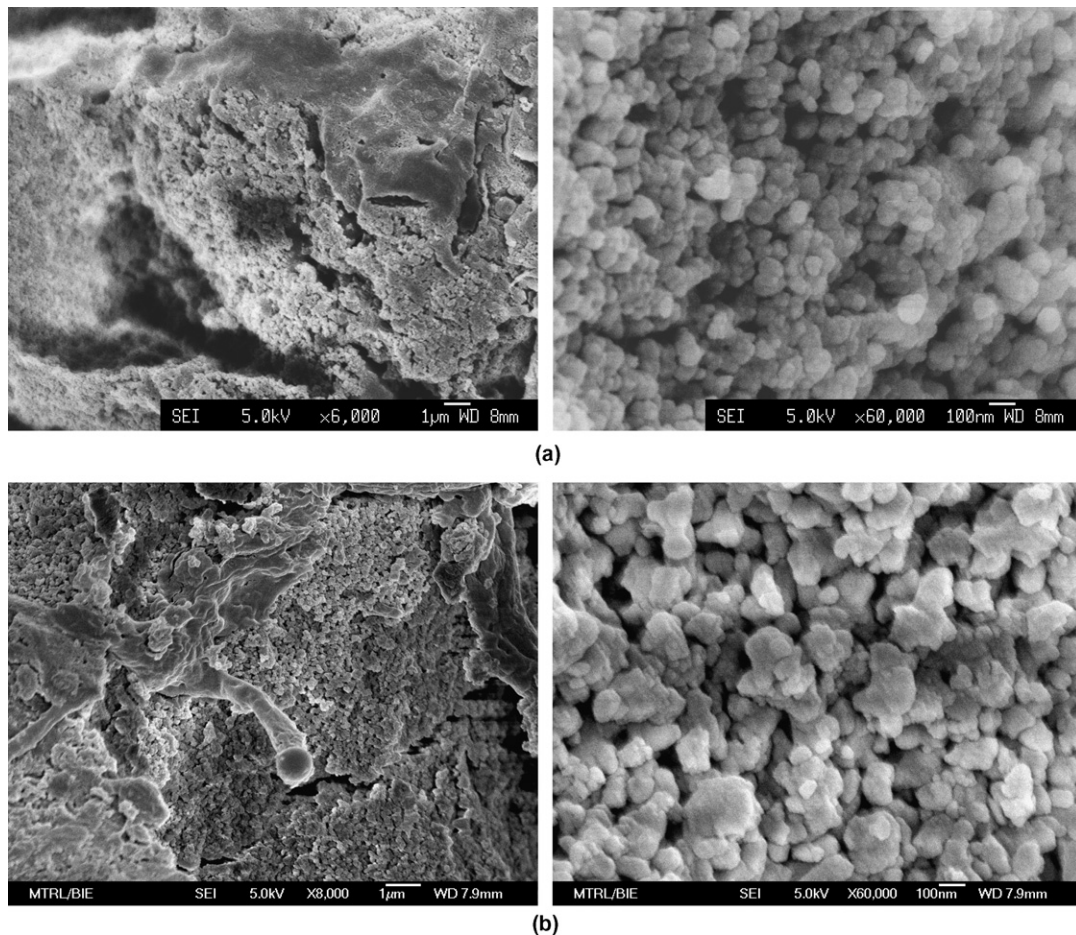


Fig. 2. Typical FESEM pictures of the HVOF coating (HVOF2, made from $40 \pm 10 \mu\text{m}$ powder) showing nanostructures at (a) their surface and (b) fractured cross-sections ((a-2) and (b-2) refer to closer observation on (a-1) and (b-1) respectively).

Table 1
 Sizes of the nano-grains in the starting powder and coatings (melted part)

Sample	Size and features of the nanosized grains (shape)		
	Coating surface	Inside coating	Near to coating/substrate interface
HVOF coating ($50 \pm 10 \mu\text{m}$)	50–100 nm (spherical: melted part)	50–100 nm (spherical: melted part)	60–120 nm (spherical: melted part)
HVOF coating ($40 \pm 10 \mu\text{m}$)	50–100 nm (spherical)	60–110 nm (spherical)	60–120 nm (spherical)
HVOF coating ($30 \pm 10 \mu\text{m}$)	50–100 nm (spherical)	50–100 nm (spherical)	Mostly: <250 nm in length, <50 nm in diameter; Rarely: 80–120 nm in width, 0.4–1.2 μm in length (hexagonal)

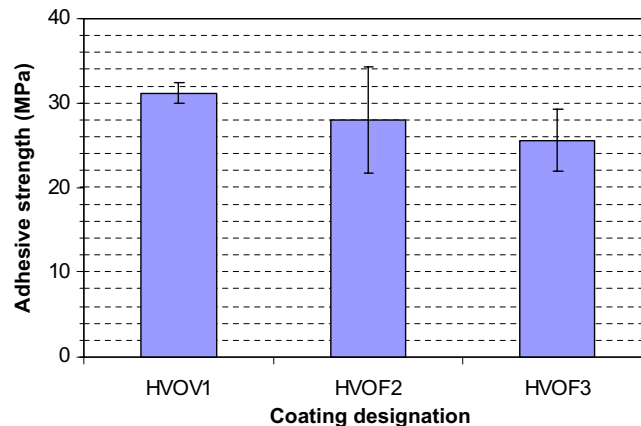


Fig. 3. Adhesive strength of the coatings (HVOF1: HA coating made from $50 \pm 10 \mu\text{m}$ powder, HVOF2: HA coating made from $40 \pm 10 \mu\text{m}$ powder, HVOF3: HA coating made from $30 \pm 10 \mu\text{m}$ powder). The error bar means standard deviation and the differences among the values are significant, $p < 0.05$, as analyzed by the paired student's t -distribution.

substrate interface. This in turn indicates that the coating/substrate interface plays a key role in determining the adhesion. FESEM observation from the bottom side of the coatings (the area with intimate contact with the substrate) shows interesting nanostructures (Fig. 4). That is, the HVOF sprayed coatings made from the smallest powder ($30 \pm 10 \mu\text{m}$) exhibit typical hexagonal structure (Fig. 4(a)). Most of the grains show similar morphological features (Fig. 4a-1) that have a size of <250 nm in length and <50 nm in diameter. Very rare of them show enlarged size of 0.4–1.2 μm in length and 80–120 nm in width (Fig. 4a-2). The formation of the nanosized grains with hexagonal prismatic morphology indicates the influence of both the melt-state and temperature of the HA particles upon their impingement. The partial melt state during HVOF spraying could result in a faster cooling rate of the molten part upon their impingement on the room-temperature substrate. The high cooling rate would influence the formation of the hexagonal grains. Even though Chraska et al. reported their findings that the top surface of the first solidified splat causes epitaxial growth of columnar grains in subsequent splats for plasma sprayed YSZ [29], the present study revealed spherical nanosized grains within the second folded splat and there is no experimental evidence of presence of columnar grains in other parts in the coatings other than in the first layer splats. The comparison among the HVOF coatings suggests a weak bonding of the hexagonal grains with the substrate (Figs. 3, 4). The perpendicular grains might have changed the residual stresses at the coating/substrate interface, or even more probably, they weakened the mechanical interlocking of the coating by the substrate. The granular nanosized grains with irregular pores could be capable of enhancing mechanical interlocking by the roughened substrate (Fig. 4b-1). It therefore indicates that formation of hexagonal grains near to the coating/substrate interface must be avoided. Sufficient substrate preheating might be an approach to achieve such purpose through decreasing the cooling rate upon the impingement of the droplets.

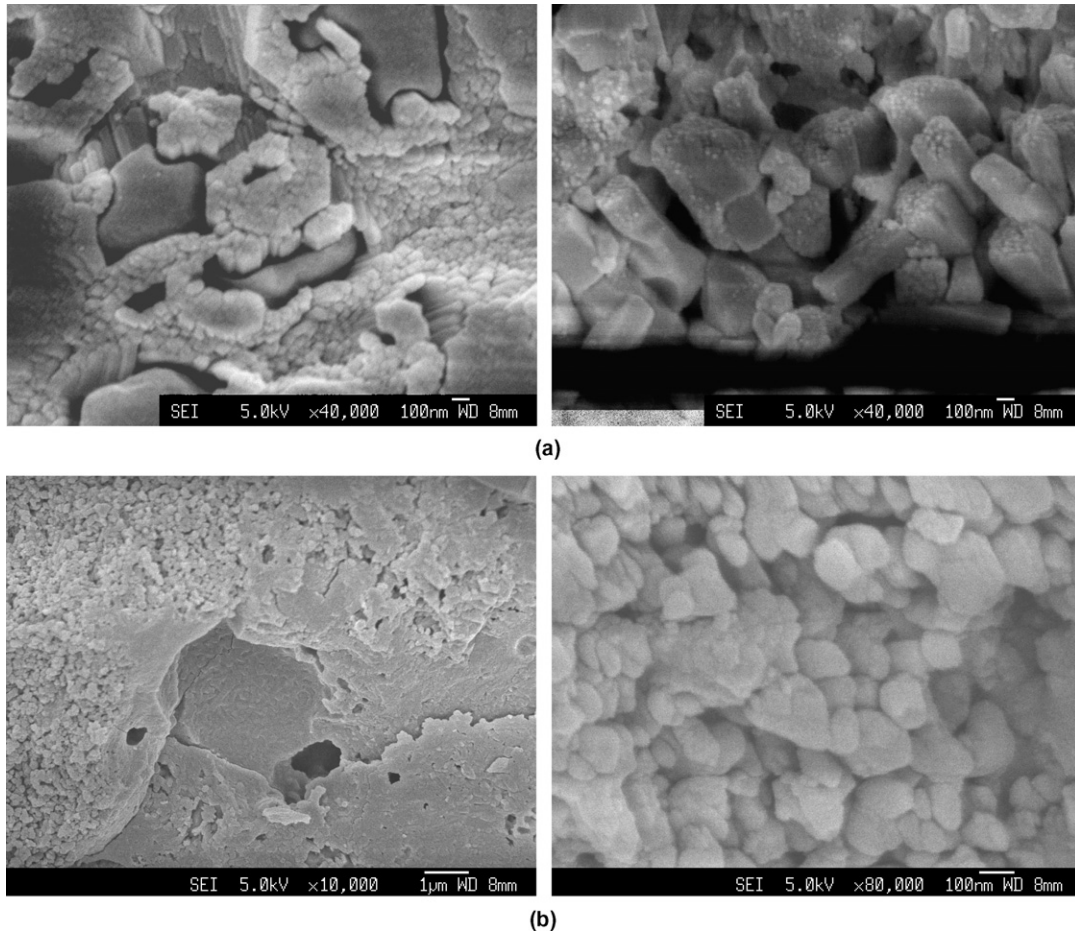


Fig. 4. Typical FESEM photos taken at the coating bottom (with intimate contact with the substrate), (a-1,2) HVOF coating made from $30 \pm 10 \mu\text{m}$ powder showing cuboid nanosized grains, (b-1,2) HVOF coating made from $40 \pm 10 \mu\text{m}$ powder showing spherical nanosized grains.

Minor difference in the G_{ss} values was found among the coatings (Fig. 5). In order to reveal the effect of coating microstructure on the G_{ss} , failure mechanism was discussed through observing the worn morphology after bending by SEM, which is typically shown in Fig. 6. It is noted that the crack induced by bending stress did not grow along the coating/substrate interface. HA coatings remained on the substrate with varied thickness from several microns to approximately 25 microns depending on the locations. The thickness is roughly equal to that of one splat or two. The crack growth mechanism has already disclosed that the crack always propagates along the direction with minimum strain energy. According to Sih [12], once a crack is initiated the fracture path follows the trajectory of points of minimum strain energy density remarkably well. Concerning the complex residual stresses and the applied stresses from bending moment at the crack front, the crack propagation into the coating side can be explained by the possible flaws, such as micropores and microcracks within the coating. Observation of the microstructure from the cross-sections of the coatings gives insight into the flaws inside the coating (Fig. 7). There is clear evidence of micro-/nanosized pores (Fig. 7(a)) and unbonded area between the HA splats. The sizes of the pores in the nanostructured HA coatings are in the range of $\sim 20\text{--}110 \text{ nm}$. These should act as the crack path and accelerate the crack propagation as well during the bending. The wave-shape-like worn surface together with the bending curve analysis, which is shown in Fig. 8, indicate that kinking and trapping of the bending cracks occurred during crack growth. Prior to entire bending failure, the decrease in the flexure load which frequently appeared is associated with the crack kinking into the coating away from the interface. The trapping of the crack in the coating subsequently occurs, then

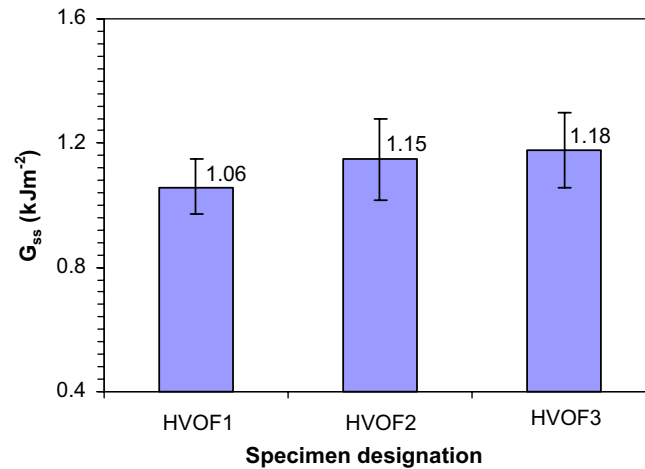


Fig. 5. Critical strain energy release rate (G_{ss}) of the HA coatings obtained from 4-point bend test. (HVOF1: HA coating made from $50 \pm 10 \mu\text{m}$ powder, HVOF2: HA coating made from $40 \pm 10 \mu\text{m}$ powder, HVOF3: HA coating made from $30 \pm 10 \mu\text{m}$ powder.)

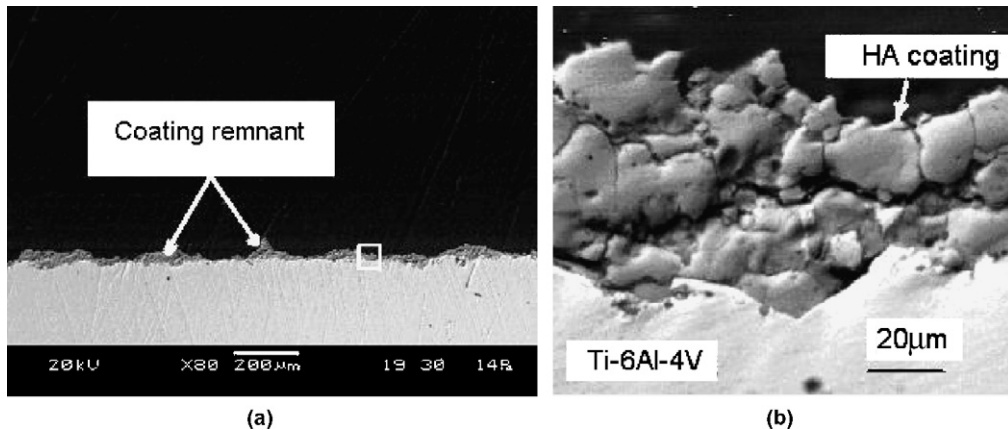


Fig. 6. Typical worn cross-sectional morphology of the HA coating after bending failure ((b) shows the magnified view of the region marked in (a)).

the crack propagates in nearly parallel direction to the coating/substrate interface. Another kinking occurs again following the former procedure. Finally, the entire failure takes place due to the large opening of a flexural crack in the specimen, which is suggested by the large drop of the load. Typical failure morphology reveals that there is no evidence of cracking parallel to the surface of lamellae. The trace of the brittle fracture suggests that the existed defects at the splats' interface might have been connected together as the propagation path of the crack. Furthermore, the size and distribution of pores also play an important role in influencing both the crack initiation and propagation processes [30], thus failure would occur when sufficient micropores have been connected by unbonded area between splats and trans-lamella microcracks to separate that region from the remainder of the coating. The effect of micropores located along the crack propagation path on the fracture toughness has been discussed by Leguillon [31]. It was believed that the crack growth was made of successive sudden jumps at each void along the crack path. Thus, the existence of micropores at the crack propagation path (splats' interface in this case) is detrimental to the fracture property. Furthermore, it has been found that the thickness of the retained coating is very much consistent with that of one splat or two. Typical topographical morphology of the first-layer splat is shown in Fig. 9. It is clear that apart from the nanosized grains, there are indeed a large amount of nanosized pores. Nevertheless, the cohesion inside individual splats is much better than that between individual HA splats, which also accounts for the bending crack

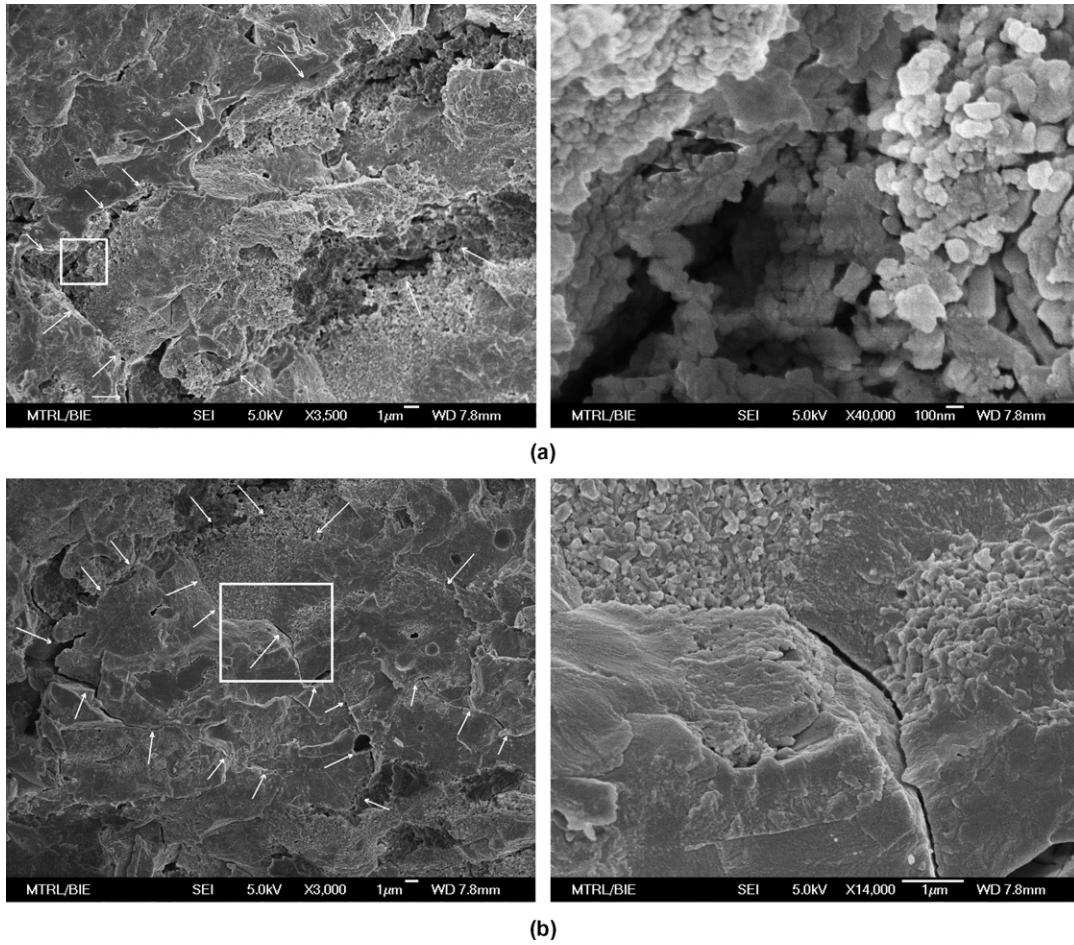


Fig. 7. FESEM pictures showing the poor bonding state between the HA splats. The photos were taken from fractured cross-sections of the coatings. (a) micro- and nanosized pores located at the splats' interface, and (b) clear unbonded interface between the splats. Arrows point to the splats' interface.

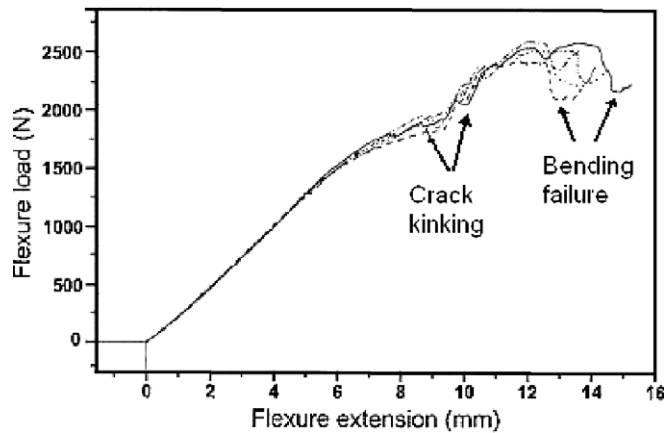


Fig. 8. Typical flexure curves of the HA coatings showing the kinking and trapping of the crack during its propagation. The five specimens were obtained from the same coating group (HVOF2).

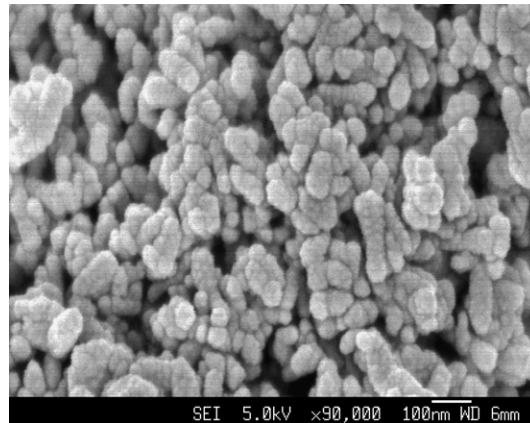


Fig. 9. FESEM picture taken from the surface of the splat showing consistent nanosized grains and nanosized pores.

propagation along the splats' interface. Since the fracture occurred within the coating, the existence of the hexagonal nanosized grains did not show obvious influence on the crack growth.

The different G_{ss} values can be well explained by the nanostructures of the coatings. The smallest HA powder particles resulted in the finest grains (Table 1), which in turn contributes to the densest coating structure (lowest porosity). Therefore, it is reasonable that the strain energy release rate of the coating made from 40 μm powder is higher than that of the coating made from 50 μm powder. Since the bending fracture took place mostly within the HA coating near to the coating/substrate interface, the fracture energy of coating/substrate interface is higher than that of HA coating. As discussed earlier, this is partially due to the large quantities of defects in the coating rather than at the interface. It is proposed that the microstructure of thermal sprayed coatings controls their toughness. In addition, it is noted that the G_{ss} value obtained in this study is relatively high. This might be partly attributable to the mode mix of the 4-point delamination test. Further refined study is required to clarify the crack propagation behavior. Even though many researchers have utilized the four-point bend test to determine the interfacial fracture toughness [14,15], the use of such technique for ceramic coatings is very much limited. It should be pointed out that this approach is not accurate for determining fracture energy of the present coatings because the formula used for the calculation of strain energy release rate is based on the assumption that the interface crack symmetrically advances during bending. Nevertheless, since the tested G_{ss} is significantly dependent on coating microstructure and the remnant coating is very thin, it is still acceptable for evaluating the coating structure.

4. Conclusions

Shape and sizes of the nanosized grains with intimate contact with the substrate affect the adhesion of the HA coatings. The hexagonal grains with enlarged sizes (e.g., upto 250 nm in side length) deteriorated the adhesion, while the granular nanosized grains enhanced the bonding of the coating through improving the interlocking by the substrate. The 4-point bend test for determining the strain energy release rate of the HA coatings revealed the weakest zone to be inside the coating near to the coating/substrate interface with the thickness of one splat or two. The bending cracks propagated along the splats' interface within the coating. The 4-point bend test was not appropriate for evaluating the coating/substrate interface properties. The HA coating with finer nanosized grains and lower porosity is suggested for achieving better fracture properties.

Acknowledgement

The author, H. Li, acknowledges the Singapore Millennium Foundation (SMF) for its post-doctoral research fellowship.

References

- [1] Suominen E, Aho AJ, Vedel E, Kangasniemi I, Uusipaikka E, Yli-Urpo A. Subchondral bone and cartilage repair with bioactive glasses hydroxyapatite and hydroxyapatite-glass composite. *J Biomed Mater Res* 1996;32:543–51.
- [2] Szivek JA, Anderson PL, Dishongh TJ, de Young DW. Evaluation of factors affecting bonding rate of calcium phosphate ceramic coatings for in vivo strain gauge attachment. *J Biomed Mater Res* 1996;33:121–32.
- [3] Shaw LL, Barber B, Jordan EH, Gell M. Measurements of the interfacial fracture energy of thermal barrier coatings. *Scripta Materialia* 1998;39:1427–34.
- [4] Piveteau LD, Girona MI, Schlapbach L, Barbous P, Boilot J-P, Gasser B. Thin films of calcium phosphate and titanium dioxide by a sol-gel route a new method for coating medical implants. *J Mater Sic Mater Med* 1999;10:161–4.
- [5] Gross KA, Ben-Nissan B, Walsh WR, Swarts E. Analysis of retrieved hydroxyapatite coated orthopaedic implants. In: Christian Coddet, editor. *Thermal spray: meeting the challenges of the 21st century*, Proceedings of the 15th international thermal spray conference, Nice, France, May 1998, p. 1133–8.
- [6] Bonfield W. New trends in implant materials. In: Pizzoferrato A, Marchetti PG, Ravaglioli A, Lee AJC, editors. *Biomaterials and clinical applications*, Proceedings of the sixth conference for biomaterials, Bologna, Italy, 1987, p. 13–21.
- [7] Krauser JT, Berthold P. A scanning electron microscopy study of failed root from dental implant. *J Dental Res* 1991;70:274–81.
- [8] Wang BC, Lee TM, Chang E, Yang CY. The shear strength and failure mode of plasma-sprayed hydroxyapatite coating to bone: The effects of coating thickness. *J Biomed Mater Res* 1993;27:1315–27.
- [9] Inadome T, Hayashi K, Nakashima Y, Tsumura H, Sugioka Y. Comparison of bone-implant interface shear strength of hydroxyapatite-coated and alumina-coated implants. *J Biomed Mater Res* 1995;29:19–24.
- [10] Hayashi K, Inadome T, Mashima T, Sugioka Y. Comparison of bone-implant interface shear strength of solid hydroxyapatite and hydroxyapatite-coated titanium implants. *J Biomed Mater Res* 1993;27:557–63.
- [11] Chung HGP, Swain MV, Mori T. Evaluation of the strain energy release rate for the fracture of titanium-porcelain interfacial bonding. *Biomaterials* 1997;18:1553–7.
- [12] Sih GC. *Mechanics of fracture initiation and propagation*. USA: Kluwer Academic Publishers; 1991.
- [13] Howard SJ, Clyne TW. Interfacial fracture toughness of vacuum-plasma-sprayed coatings. *Surf Coat Technol* 1991;45:333–42.
- [14] Howard SJ, Phillips AJ, Clyne TW. The interpretation of data from the four-point bend delamination test to measure interfacial fracture toughness. *Composites* 1993;24:103–12.
- [15] Howard SJ, Tsui YC, Clyne TW. The effect of residual stresses on the debonding of coatings-I: A model for delamination at a bimaterial interface. *Acta Metall Mater* 1994;42:2823–36.
- [16] Haman JD, Chittur KK. Four point bend testing of calcium phosphate coatings, In: *Proceedings of 16th southern biomedical engineering conference*, 1997, p. 305–8.
- [17] Zhu YC, Yukimura K, Ding CX, Zhang PY. Tribological properties of nanostructured and conventional WC–Co coatings deposited by plasma spraying. *Thin Solid Films* 2001;388:277–82.
- [18] Berndt CC, editor. *Thermal spray processing of nanoscale materials II – extended abstracts*. *J Therm Spray Technol* 2001;10:147–80.
- [19] Tjong SC, Chen H. Nanocrystalline materials coatings. *Mater Sci Eng R: Reports* 2004;45:1–88.
- [20] Li JF, Liao H, Wang XY, Coddet C, Chen H, Ding CX. Plasma spraying of nanostructured partially yttria stabilized zirconia powders. *Thin Solid Films* 2004;460:101–15.
- [21] Gell M, Jordan EH, Sohn YH, Goberman D, Shaw L, Xiao TD. Development and implementation of plasma sprayed nanostructured ceramic coatings. *Surf Coat Technol* 2001;146:48–54.
- [22] Gutwein LG, Webster TJ. Increased viable osteoblast density in the presence of nanophase compared to conventional alumina and titania particles. *Biomaterials* 2004;25:4175–83.
- [23] Webster TJ, Siegel RW, Bizios R. Osteoblast adhesion on nanophase ceramics. *Biomaterials* 1999;20:1221–7.
- [24] Clyne TW, Gill SC. Residual stresses in thermal spray coatings and their effect on interfacial adhesion: a review of recent work. *J Therm Spray Technol* 1996;5:401–18.
- [25] Charalambides PG, Lund J, Evans AG, McMeeking RM. A test specimen for determining the fracture resistance of bimaterial interfaces. *J Appl Mech* 1989;56:77–82.
- [26] Murakami Y. chief editor, *Stress intensity factors handbook*, vol. 3, Committee on fracture mechanics. Soc Mater Sci, Japan, 1992.
- [27] Evans AG, Ruhle M, Dalgleish BJ, Charalambides PG. The fracture energy of bimaterial interfaces. *Mat Sci Eng* 1990;A126:53–64.
- [28] Li H, Khor KA, Cheang P. Properties of heat-treated calcium phosphate coatings deposited by high-velocity oxy-fuel (HVOF) spray. *Biomaterials* 2002;23:2105–12.
- [29] Chraska T, King AH. Transmission electron microscopy study of rapid solidification of plasma sprayed zirconia – Part II. Interfaces and subsequent splat solidification. *Thin Solid Films* 2001;397:40–8.
- [30] Ishihara S, Mcevely AJ, Goshima T, Kanekasu K, Nara T. On fatigue lifetimes and fatigue crack growth behavior of bone cement. *J Mater Sci Mater Med* 2000;11:661–6.
- [31] Leguillon D. Influence of micro-voids on toughness of interfaces. In: Rossmannith H, editor. *Damage and failure of interface*. Rotterdam: Balkema; 1997. p. 113–20.